Verification of high-order mixed FEM solution of transient Magnetic diffusion problems

R. Rieben, D. A. White

May 19, 2005

Disclaimer

This document was prepared as an account of work sponsored by an agency of the United States Government. Neither the United States Government nor the University of California nor any of their employees, makes any warranty, express or implied, or assumes any legal liability or responsibility for the accuracy, completeness, or usefulness of any information, apparatus, product, or process disclosed, or represents that its use would not infringe privately owned rights. Reference herein to any specific commercial product, process, or service by trade name, trademark, manufacturer, or otherwise, does not necessarily constitute or imply its endorsement, recommendation, or favoring by the United States Government or the University of California. The views and opinions of authors expressed herein do not necessarily state or reflect those of the United States Government or the University of California, and shall not be used for advertising or product endorsement purposes.

Verification of High-Order Mixed FEM Solution of Transient Magnetic Diffusion Problems

R. Rieben   and D. White

Abstract—

We develop and present high order mixed finite element discretizations of the time dependent electromagnetic diffusion equations for solving eddy current problems on 3D unstructured grids. The discretizations are based on high order H(grad), H(curl) and H(div) conforming finite element spaces combined with an implicit and unconditionally stable generalized Crank-Nicholson time differencing method. We develop three separate electromagnetic diffusion formulations, namely the $\vec{E}$ (electric field), $\vec{H}$ (magnetic field) and the $\vec{A}$-φ (potential) formulations. For each formulation, we also provide a consistent procedure for computing the secondary variables $\vec{J}$ (current flux density) and $\vec{B}$ (magnetic flux density), as these fields are required for the computation of electromagnetic force and heating terms. We verify the error convergence properties of each formulation via a series of numerical experiments on canonical problems with known analytic solutions. The key result is that the different formulations are equally accurate, even for the secondary variables $\vec{J}$ and $\vec{B}$, and hence the choice of which formulation to use depends mostly upon relevance of the Natural and Essential boundary conditions to the problem of interest. In addition, we highlight issues with numerical verification of finite element methods which can lead to false conclusions on the accuracy of the methods.

Index Terms—

Computational electromagnetics, Maxwell's equations, vector finite elements, high order methods, $H(Curl)$ and $H(Div)$ - conforming methods, discrete differential forms, transient eddy currents, electromagnetic diffusion

I. INTRODUCTION

In this paper we present high order mixed finite element formulations for solving the time dependent electromagnetic diffusion equations. Various formulations for these equations exist and have been extensively reviewed and studied in the literature. These include formulations which solve for the electric field (the $\vec{E}$ field formulation) [1], [2], [3], the magnetic field (the $\vec{H}$ field formulation) [4], [5] or for the potential field (the $\vec{A}$-φ potential formulation) [6], [7], [8], [9]. Each formulation has its advantages and disadvantages for problems in computational electromagnetics. However, we show that when using $H(Curl)$ and $H(Div)$ conforming finite element methods there is no difference in *accuracy* for these three formulations, even for secondary quantities such as $\vec{B}$ and $\vec{J}$. This is in contrast to the often believed premise that there will be a loss in accuracy

when computing $\vec{B}$ from $\vec{\nabla} \times \vec{A}$ or computing $\vec{J}$ from $\vec{\nabla} \times \vec{H}$. The difference between the three formulations, which use primary field variables $\vec{E}, \vec{H}$, and $\vec{A}$, respectively, is in the boundary conditions and the source terms, and is therefore simply a matter of which formulation is most convenient for a given electromagnetics problem.

The most difficult electromagnetic diffusion problems encountered in practice are those that involve multiple conductors separated by a non-conducting region, the so-called multiply connected eddy current problem. While the currents are zero in the non-conducting region clearly the fields are not, and some method must be used to account for these fields. One approach is to simply mesh the non-conducting region and use a small value of conductivity in this region. While seemingly a crude approach, it works well in practice for many problems, for example using a conductivity at least 10^3 times smaller than the metal results in fields correct to within the discretization error [7], [10]. The difficulty is the solve time due to the large number of unknowns and matrix ill-conditioning. More sophisticated approaches include solving a magnetostatic problem in the non-conducing region and coupling the the two solutions (the coupled approach), or employing an integral equation to correctly model the global boundary condition (the hybrid FEM/BEM approach). While we do provide a computational example where we employ a conductivity contrast of 10^7, which can be considered an approximation to air or vacuum, in this paper we do not advocate any particular approach for dealing with non-conducting regions.

Here we review high order mixed finite element spatial discretizations of each of the previously mentioned formulations. In the context of Galerkin approximations, the choice of the finite element space plays a crucial role in the stability and convergence of the discretization. For instance, in numerical approximations of the magnetic and electric field intensities, $H(Curl)$ conforming finite element spaces (or edge elements) are preferred over traditional nodal vector spaces since they eliminate spurious modes in eigenvalue computations and they prevent fictitious charge build-up in time-dependent computations. The lowest order $H(Curl)$ conforming basis functions were developed by Whitney [11] before the advent of finite element programs. Arbitrary order versions were introduced by Nédélec [12], [13] as a generalization of the mixed finite element spaces introduced by P.A. Raviart and J.M. Thomas [14] for $H(Div)$ conforming methods. Application of these $H(Curl)$ and $H(Div)$ basis functions toward electromagnetics is becoming quite popular and applications can be found in several recent textbooks [15], [5], [16]

A numerical implementation of arbitrary order $H(Curl)$ and

$H(Div)$ basis functions can be found in the finite element software library FEMSTER [17]. This specific implementation has been rigorously verified in the context of high order finite element solutions to transient wave equations and it has been shown that such a formulation can drastically reduce the effects of numerical dispersion, [18], [19]. Higher-order basis functions can be combined with high order energy conserving time integration schemes for further gains in accuracy [20], [19].

In this paper we apply a rigorous verification process of high order mixed FEM solutions of the electromagnetic diffusion equations. We define the verification process in a manner similar to [21] where five essential points of numerical verification are presented. These include:

- Comparing code results to a related problem with an exact answer
- Establishing that the convergence rate of the truncation error with changing grid spacing is consistent with expectations
- Comparing calculated with expected results for a problem specially manufactured to test the code
- Monitoring conserved quantities and parameters, preservation of symmetry properties, and other easily predictable outcomes
- Benchmarking – that is, comparing results with those from existing codes that can calculate similar problems

It is important to distinguish *verification* from *validation*. Verification is concerned with numerical methods and the software implementation of these methods. In the context of finite element methods verification answers the question "Is the given Initial Boundary Value Problem (the PDE + boundary conditions + material models) being solved correctly?" Validation, on the other hand, is concerned with the validity of the given Initial Boundary Value Problem for a specific problem or set of problems. Validation answers the question "To what extent does this simulation agree with physical reality?" For example, one may question the validity of the diffusion approximation (neglecting displacement current) in the first place [22], or one may question validity of assuming $\vec{H} = 0$ on a particular boundary. We will not discuss validation here.

Our verification examples are carefully constructed to illustrate some issues with numerical verification of finite element methods. We show cases where computational results are super-convergent (better than expected) and sub-convergent (worse than expected), highlighting the fact that the true performance of a method cannot be ascertained by a single computational experiment.

II. ELECTROMAGNETIC DIFFUSION EQUATIONS

When working with multiple finite element spaces, it becomes convenient to use the notation of differential forms as a way of categorizing the various field quantities from Maxwell's equations and the subsequent finite element spaces used to discretize them. In addition, the calculus of differential forms provides the necessary transformation rules which allow complicated basis functions to be derived on a reference element and then mapped to global mesh elements. Table I lists various physical quantities in electromagnetics and their associated differential form.

Physical Quantity	Units	Diff. Form
Scalar Potential, ϕ	*Volts/m^0*	0-form
Vector Potential, $\vec{A}$	*Webbers/m^1*	1-form
Electric Field Intensity, $\vec{E}$	*Volts/m^1*	1-form
Magnetic Field Intensity, $\vec{H}$	*Amps/m^1*	1-form
Electric Flux Density, $\vec{D}$	*Coulombs/m^2*	2-form
Magnetic Flux Density, $\vec{B}$	*Webbers/m^2*	2-form
Electric Charge Density, ρ	*Coulombs/m^3*	3-form

TABLE I

ELECTROMAGNETIC QUANTITIES AND THEIR ASSOCIATED DIFFERENTIAL FORMS

In electromagnetics we have the electric and magnetic fields $\vec{E}$, $\vec{H}$, the electric and magnetic flux densities $\vec{D}$, $\vec{B}$, and the constitutive relations

$$\vec{D} = \varepsilon \vec{E}$$
$$\vec{B} = \mu \vec{H}$$

Here we write Maxwell's Equations in terms of $\vec{E}$ and $\vec{B}$,

$$\varepsilon \frac{\partial \vec{E}}{\partial t} = \vec{\nabla} \times \frac{1}{\mu} \vec{B} - \sigma \vec{E} - \vec{J}_s \tag{1}$$

$$\frac{\partial \vec{B}}{\partial t} = -\vec{\nabla} \times \vec{E} \tag{2}$$

$$\vec{\nabla} \cdot \varepsilon \vec{E} = 0 \tag{3}$$

$$\vec{\nabla} \cdot \vec{B} = 0 \tag{4}$$

with appropriate boundary conditions and initial conditions understood. Note that $\vec{J}_s$ is an independent current source term, which may or may not exist for every problem. In all of our subsequent formulations, the material properties ε, μ, σ are free to be symmetric positive definite tensor functions of space, but we impose the restriction that they are independent of time.

Now consider solving Maxwell's Equations within a good conductor. A good conductor is defined by the condition

$$\varepsilon \frac{\partial \vec{E}}{\partial t} \ll \sigma \vec{E}. \tag{5}$$

Note that (5) depends not only on the material properties σ and ε, but also on the time rate of change of $\vec{E}$. When (5) is satisfied, Maxwell's equations can be simplified by neglecting the $\varepsilon \frac{\partial \vec{E}}{\partial t}$ term altogether, this is the so-called low-frequency approximation, diffusion approximation or eddy-current approximation. The diffusion approximation is not valid for most RF, microwave, or optics problems, but is reasonable for low-frequency EM waves in plasmas or in the earth [23], [24] [25], [26], as well as for quasi-magnetostatic problems such as electric motors, transformers, induction heating, and electromagnetic rail-guns. A detailed, mathematical analysis which justifies the approximation is given in [22].

A. The $\vec{E}$ Field Formulation

Combining the Ampere-Faraday laws of (1) and (2) and applying the low-frequency approximation of (5) yields a diffusion equation for the electric field. Given the electric field, the magnetic flux and eddy current densities can be computed as well. Consider a 3 dimensional domain Ω with surface boundary Γ, the electric field diffusion formulation is then given by

$$\sigma \frac{\partial \vec{E}}{\partial t} = -\vec{\nabla} \times \frac{1}{\mu} \vec{\nabla} \times \vec{E} - \frac{\partial \vec{J}_s}{\partial t} \tag{6}$$

$$\frac{\partial \vec{B}}{\partial t} = -\vec{\nabla} \times \vec{E} \tag{7}$$

$$\vec{J} = \sigma \vec{E} \tag{8}$$

For this paper, we consider two different types of boundary conditions, namely the essential (or inhomogeneous Dirichlet) boundary condition

$$\hat{n} \times \vec{E} = \vec{E}_{tan} \ \text{on} \ \Gamma \tag{9}$$

and the natural (or homogeneous Neumann) boundary condition

$$\hat{n} \times \frac{1}{\mu} \vec{\nabla} \times \vec{E} = 0 \ \text{on} \ \Gamma \tag{10}$$

There are divergence constraints on both the primary and secondary fields, namely

$$\vec{\nabla} \cdot \sigma \vec{E} = 0 \tag{11}$$

$$\vec{\nabla} \cdot \vec{B} = 0 \tag{12}$$

B. The $\vec{H}$ Field Formulation

The magnetic field diffusion equation can be derived by again combining (1) and (2) and applying the low-frequency approximation, this time eliminating $\vec{E}$ instead of $\vec{B}$,

$$\mu \frac{\partial \vec{H}}{\partial t} = -\vec{\nabla} \times \frac{1}{\sigma} \vec{\nabla} \times \vec{H} + \frac{1}{\sigma} \vec{\nabla} \times \vec{J}_s \tag{13}$$

$$\vec{B} = \mu \vec{H} \tag{14}$$

$$\vec{J} = \vec{\nabla} \times \vec{H} - \vec{J}_s \tag{15}$$

The essential (inhomogeneous Dirichlet) boundary condition is given by

$$\hat{n} \times \vec{H} = \vec{H}_{tan} \ \text{on} \ \Gamma \tag{16}$$

while the natural (homogeneous Neumann) boundary condition is given by

$$\hat{n} \times \frac{1}{\sigma} \vec{\nabla} \times \vec{H} = 0 \ \text{on} \ \Gamma \tag{17}$$

There are divergence constraints on both the primary and secondary fields, namely

$$\vec{\nabla} \cdot \mu \vec{H} = 0 \tag{18}$$

$$\vec{\nabla} \cdot \vec{J} = 0 \tag{19}$$

C. The $\vec{A}$-ϕ Potential Formulation

The divergence condition (4) implies that $\vec{B} = \vec{\nabla} \times \vec{A}$ where $\vec{A}$ is a magnetic vector potential. This in turn implies that the electric field is given by $\vec{E} = -\vec{\nabla}\Phi - \frac{\partial}{\partial t}\vec{A}$, where Φ is an electric scalar potential. Using these two potentials, along with the gauge condition $\vec{\nabla} \cdot \sigma \vec{A} = 0$, the potential diffusion equations in a 3 dimensional domain Ω are

$$\vec{\nabla} \cdot \sigma \vec{\nabla} \phi = 0 \tag{20}$$

$$\sigma \frac{\partial \vec{A}}{\partial t} = -\vec{\nabla} \times \frac{1}{\mu} \vec{\nabla} \times \vec{A} - \sigma \vec{\nabla}\phi + \vec{J}_s \tag{21}$$

$$\vec{E} = -\vec{\nabla}\phi - \frac{\partial}{\partial t}\vec{A} \tag{22}$$

$$\vec{B} = \vec{\nabla} \times \vec{A} \tag{23}$$

$$\vec{J} = \sigma \vec{E} \tag{24}$$

Note that this formulation has an additional elliptic PDE (20) to solve for the scalar potential. The essential (inhomogeneous Dirichlet) boundary conditions are given by

$$\phi = \phi_{surf} \ \text{on} \ \Gamma \tag{25}$$

$$\hat{n} \times A = A_{tan} \ \text{on} \ \Gamma \tag{26}$$

while the natural (homogeneous Neumann) boundary conditions are given by

$$\hat{n} \cdot \vec{\nabla}\phi = 0 \ \text{on} \ \Gamma \tag{27}$$

$$\hat{n} \times \frac{1}{\mu} \vec{\nabla} \times A = 0 \ \text{on} \ \Gamma \tag{28}$$

Again, there are divergence constraints on both the primary and secondary fields, namely

$$\vec{\nabla} \cdot \sigma \vec{A} = 0 \tag{29}$$

$$\vec{\nabla} \cdot \vec{B} = 0 \tag{30}$$

It is interesting to note that in the potential diffusion equation we explicitly see the Helmholtz decomposition of the electric field

$$\vec{E} = \vec{E}_{irr} + \vec{E}_{sol}$$

where $\vec{E}_{irr} = -\vec{\nabla}\phi$ and $\vec{E}_{sol} = -\frac{\partial A}{\partial t}$. The total current is

$$\vec{J} = \sigma \vec{E} = \sigma \left(-\vec{\nabla}\phi - \frac{\partial \vec{A}}{\partial t} \right)$$

where the first term is irrotational and is determined solely by the boundary conditions on ϕ, and the second term is solenoidal and satisfies the diffusion equation.

The $\vec{E}$ field, $\vec{H}$ field, and $\vec{A}$-ϕ field formulations are remarkably similar. Each formulation involves a divergence constraint on the primary field of the form $\vec{\nabla} \cdot \alpha \vec{X}$, where $\vec{X}$ is the primary field variable and α is a material property. Fortunately this divergence constraint will be satisfied, automatically, by the finite element method. Each formulation involves computation of secondary fields from a curl equation $\vec{Y} = \vec{\nabla} \times \vec{X}$ where $\vec{X}$ is the primary variable and $\vec{Y}$ is the secondary variable. The $\vec{A}$-ϕ

formulation involves an additional Laplacian for ϕ and hence will be more computationally expensive to solve. But this particular formulation is well suited for problems driven by an applied voltage source, as the voltage appears explicitly in the equations.

III. SPATIAL FINITE ELEMENT DISCRETIZATION

FEMSTER is a class library of higher-order discrete differential forms that is used within the *EMSolve* CEM code [27], [17], [28]. It provides discrete numerical implementations of the concepts from differential forms (tangent vectors, wedge product, exterior derivative, hodge-star operator, etc...). In standard finite element language, FEMSTER contains all the data structures and operations required to compute local finite element matrices: elements (tetrahedrons, hexahedrons, prisms), basis functions (or shape functions), quadrature rules, linear forms, and bilinear forms. FEMSTER provides the gradient, curl, and divergence operators, as well as the, div-grad, curl-curl, and grad-div operators. Note that arbitrary partial derivative operators are not included, as these do not fit nicely into the framework of differential forms, and fortunately are not needed for computational electromagnetics. The basis function class hierarchy contains four forms of basis functions, simply called 0-forms, 1-forms, 2-forms, and 3-forms. Derived from each of these classes are sub-class for the element types tetrahedron, hexahedron, and prism, and derived from each of these types is a further specialization for the degrees-of-freedom, i.e. interpolatory, spectral, hierarchical, etc. The critical step in using FEMSTER is to decide what form should be used for each physical quantity. The essential properties of the forms are now summarized.

0-forms are continuous scalar basis functions that have a well-defined gradient. These basis functions are a finite subspace of $H(Grad)$ and are suitable for discretization of the electric potential ϕ, temperature T, etc. The basis functions are dimensionless, hence the degrees-of-freedom have the same units as the field being approximated. If the field is temperature, the degrees-of-freedom have units of temperature. The gradient of a 0-form basis function can be represented, exactly, as a combination of 1-form basis functions, i.e. $dW^0 \subset \vec{W}^1$.

1-forms are vector basis functions with continuous tangential components across elements, but discontinuous normal components. They have a well defined curl, but do not have a well defined divergence. These basis functions are a finite subspace of $H(Curl)$. The basis functions have units of m^{-1}. For example the electric field has units of $Volts/m$ and the degrees-of-freedom will therefore have units of $Volts$. It is a simple matter to integrate 1-forms along the edges of a mesh, but surface integrals are not well defined. These basis functions are ideally suited for the electric field $\vec{E}$, the magnetic field $\vec{H}$, the magnetic vector potential $\vec{A}$, etc. The curl of a 1-form basis function can be represented, exactly, as a combination of 2-form basis functions, i.e. $d\vec{W}^1 \subset \vec{W}^2$. The null space of the curl operator on 1-forms is, exactly, the space of gradients of 0-forms, $d\vec{W}^1 = 0$ implies $\vec{W}^1 = dW^0$, for simply-connected regions.

2-forms are vector basis functions with continuous normal components across elements, but discontinuous tangential components. They have a well defined divergence, but do not have a well defined curl. These basis functions are a finite subspace of $H(Div)$. The basis functions have units of m^{-2}. For example the electric current density has units of $Amperes/m^2$, therefore the degrees-of-freedom have units of $Amperes$. It is a simple matter to integrate 2-forms over surfaces of a mesh, but line integrals are not well defined. These basis functions are ideally suited for the electric flux density $\vec{D}$, the magnetic flux density $\vec{B}$, current flux density $\vec{J}$, etc. The divergence of a 2-form basis function can be represented, exactly, as a combination of 3-form basis functions. The null space of the divergence operator on 2-forms is, exactly, the space of curls of 1-forms.

3-forms are discontinuous scalar basis functions. They can't be differentiated. They can be integrated over a volume, but not over a surface or a line. These basis functions are a finite subspace of L^2. The basis functions have units of m^{-3}. For example, charge density has units of $Coulombs/m^3$ and the degrees-of-freedom will therefore have units of $Coulombs$. These basis functions are ideally suited for the electric charge density ρ, the energy density ε, etc.

A. Variational Formulation

The assumption is that we have a conforming unstructured finite element mesh composed of either tetrahedrons, hexahedrons, or prisms. We begin with the electric field formulation, the other formulations will follow similarly. The *EMSolve* philosophy is that the electric field $\vec{E}$ is a 1-form and hence is approximated using 1-form basis functions,

$$\vec{E}(x,y,z,t) \approx \sum_{i=1}^{n} e_i(t) \vec{W}_i^1(x,y,z), \qquad (31)$$

with e_i the ith degree-of-freedom and $\vec{W}^1_i$ is the ith 1-form basis function. In *EMSolve* the 1-form basis functions have units of m^{-1}, hence the degrees-of-freedom have units of $Volts$. We multiply the electric diffusion equation by a test function $\vec{W}_j^1$, integrate over the domain Ω, and then utilize Greens First Vector Theorem. Ignoring the source terms and boundary conditions for clarity, we have

$$\sigma \frac{\partial \vec{E}}{\partial t} = -\vec{\nabla} \times \frac{1}{\mu} \vec{\nabla} \times \vec{E}$$

$$\int_{\Omega} \sigma \frac{\partial \vec{E}}{\partial t} \cdot \vec{W}_j^1 \, d\Omega = -\int_{\Omega} \vec{\nabla} \times \frac{1}{\mu} \vec{\nabla} \times \vec{E} \cdot \vec{W}_j^1 \, d\Omega$$

$$\int_{\Omega} \sigma \frac{\partial \vec{E}}{\partial t} \cdot \vec{W}_j^1 \, d\Omega = -\int_{\Omega} \frac{1}{\mu} \vec{\nabla} \times \vec{E} \cdot \vec{\nabla} \times \vec{W}_j^1 \, d\Omega$$

Inserting the basis function expansion (31) for the electric field, and interchanging summation and integration, gives

$$\sum_{i=1}^{n} \int_{\Omega} \sigma \vec{W}_i^1 \cdot \vec{W}_j^1 \, d\Omega \, \frac{\partial e_i}{\partial t} = -\sum_{i=1}^{n} \int_{\Omega} \vec{\nabla} \times \vec{W}_i^1 \cdot \vec{\nabla} \times \vec{W}_j^1 \, d\Omega \, e_i$$

$$\mathbf{M} \frac{\partial}{\partial t} \mathbf{e} = -\mathbf{S}\mathbf{e}$$

where $\mathbf{M}$ and $\mathbf{S}$ are the "mass" and "stiffness" matrices, respectively, and $\mathbf{e}$ is the vector of degrees-of-freedom.

The magnetic flux density update requires computing the curl of the electric field. The *EMSolve* philosophy is that the magnetic flux density $\vec{B}$ is a 2-form and hence is approximated using 2-form basis functions,

$$\vec{B}(x,y,z,t) \approx \sum_{i=1}^{n} b_i(t)\, \vec{W}_i^2(x,y,z), \qquad (32)$$

with b_i the ith degree-of-freedom and $\vec{W}_i^2$ is the ith 2-form basis function. A key property of discrete differential forms basis functions is that the inclusion relation $dW^1 \subset W^2$ is satisfied at the discrete level, for every basis function $\vec{W}_j^1$ there exist coefficients k_{ij} such that $\sum_{k=1}^{r} k_{kj}\vec{W}_k^2 = \vec{\nabla} \times \vec{W}_j^1$. Using this fact Amperes' Law becomes

$$\frac{\partial \vec{B}}{\partial t} = -\vec{\nabla} \times \vec{E}$$

$$\sum_{i=1}^{n} \vec{W}_i^2 \frac{\partial}{\partial t} b_i = -\sum_{j=1}^{m} \vec{\nabla} \times \vec{W}_j^1 e_j$$

$$\sum_{i=1}^{n} \vec{W}_i^2 \frac{\partial}{\partial t} b_i = -\sum_{j=1}^{m} \left[\sum_{k=1}^{r} k_{kj}\vec{W}_k^2 \right] e_j$$

$$\sum_{i=1}^{n} \vec{W}_i^2 \frac{\partial}{\partial t} b_i = -\sum_{i=1}^{n} \vec{W}_i^2 \sum_{j=1}^{m} k_{ij} e_j$$

$$\frac{\partial}{\partial t}\mathbf{b} = -\mathbf{K}\mathbf{e}$$

where $\mathbf{K}$ is a rectangular $n \times m$ matrix, with r non-zero entries per column, that maps 1-form degrees-of-freedom to 2-form degrees-of-freedom, and is the matrix version of the relation $dW^1 \subset W^2$. For lowest order basis functions, $\mathbf{K}$ is the mesh edge-face incidence matrix, for higher-order basis functions the matrix $\mathbf{K}$ must be computed.

The divergence constraint on the electric field will be satisfied in the weak sense. The divergence equation is multiplied by a 0-form test function W^0, the result is integrated over the domain Ω, and integration-by-parts moves the derivative to the test function,

$$\vec{\nabla} \cdot \sigma\vec{E} = 0$$

$$\int_{\Omega} \vec{\nabla} \cdot \sigma\vec{E} W_j^0 = 0$$

$$\int_{\Omega} \sigma\vec{E} \cdot \vec{\nabla} W_j^0 = 0$$

Inserting the basis function expansion (31) for the electric field, and interchanging summation and integration, gives

$$\sum_{i=1}^{n} \left[\int_{\Omega} \sigma\vec{W}_i^1 \cdot \vec{\nabla} W_j^0 \right] e_i = 0$$

$$\mathbf{D}^T \mathbf{e} = 0$$

where $\mathbf{D}^T$ is a rectangular matrix representing the divergence of a 1-form field. For lowest order basis functions, this matrix maps edges to nodes, and the constraint is equivalent to stating that the sum of the fields entering a node is zero.

The divergence constraint on the magnetic flux density will be satisfied in the strong sense. If the magnetic charge density

were non-zero, it would be considered a 3-form, hence the divergence operator is a matrix that maps 2-form fields to 3-form fields. A key property of discrete differential forms basis functions is that the inclusion relation $dW^2 \subset W^3$ is satisfied at the discrete level, for every basis function $\vec{W}_i^2$ there exist coefficients q_{ki} such that $\sum_{k=1}^{r} q_{ki}W_k^3 = \vec{\nabla} \cdot \vec{W}_i^2$. Using this relation gives

$$\vec{\nabla} \cdot \vec{B} = 0$$

$$\sum_{i=1}^{n} \vec{\nabla} \cdot \vec{W}_i^2 b_i = \sum_{j=1}^{m} W_j^3 \rho_j = 0$$

$$\sum_{i=1}^{n} \left[\sum_{k=1}^{r} q_{ki}W_k^3 \right] b_i = \sum_{j=1}^{m} W_j^3 \rho_j = 0$$

$$\sum_{j=1}^{m} W_k^3 \sum_{i=1}^{n} q_{ji} b_i = \sum_{j=1}^{m} W_j^3 \rho_j = 0$$

$$\mathbf{Q}\mathbf{b} = 0$$

where $\mathbf{Q}$ is a rectangular $n \times m$ matrix, with r non-zero entries per column, representing the divergence of a 2-form matrix, and is a discrete version of the relation $dW^2 \subset W^3$. For lowest order basis functions, $\mathbf{Q}$ is the mesh face-cell incidence matrix, and the divergence constraint is equivalent to stating that the sum of the fluxes entering a cell is zero.

For the $\vec{H}$ field and $\vec{A}$ field formulations the primary field is also a 1-form, and this results in similar mass and stiffness matrices, the only difference being the material properties used. For each formulation, the secondary fields $\vec{B}$ and $\vec{J}$ are approximated using 2-form basis function expansions. In addition, it is necessary to define matrices for constitutive equations such as $\vec{J} = \sigma\vec{E}$ and $\vec{B} = \mu\vec{H}$, which also map 1-forms to 2-forms. All of these matrices are defined below.

B. Local Finite Element Operation

FEMSTER computes the following "mass", "stiffness", and "derivative" matrices, where the superscript 0,1,2,3 denotes the degree of the form,

$$\mathbf{M}^0(\alpha)_{ij} = \int_{\Omega} \alpha W_i^0 W_j^0 \, d\Omega \qquad (33)$$

$$\mathbf{M}^1(\alpha)_{ij} = \int_{\Omega} \alpha W_i^1 \cdot W_j^1 \, d\Omega \qquad (34)$$

$$\mathbf{M}^2(\alpha)_{ij} = \int_{\Omega} \alpha W_i^2 \cdot W_j^2 \, d\Omega \qquad (35)$$

$$\mathbf{M}^3(\alpha)_{ij} = \int_{\Omega} \alpha W_i^3 W_j^3 \, d\Omega \qquad (36)$$

$$\mathbf{S}^0(\alpha)_{ij} = \int_{\Omega} \alpha \vec{\nabla} W_i^0 \cdot \vec{\nabla} W_j^0 \, d\Omega \qquad (37)$$

$$\mathbf{S}^1(\alpha)_{ij} = \int_{\Omega} \alpha \vec{\nabla} \times W_i^1 \cdot \vec{\nabla} \times W_j^1 \, d\Omega \qquad (38)$$

$$\mathbf{S}^2(\alpha)_{ij} = \int_{\Omega} \alpha \vec{\nabla} \cdot W_i^2 \, \vec{\nabla} \cdot W_j^2 \, d\Omega \qquad (39)$$

$$\mathbf{D}^{01}(\alpha)_{ij} = \int_{\Omega} \alpha \vec{\nabla} W_i^0 \cdot W_j^1 \, d\Omega \qquad (40)$$

$$\mathbf{D}^{12}(\alpha)_{ij} = \int_{\Omega} \alpha \vec{\nabla} \times W_i^1 \cdot W_j^2 \, d\Omega \qquad (41)$$

$$\mathbf{D}^{23}(\alpha)_{ij} = \int_{\Omega} \alpha \vec{\nabla} \cdot W_i^2 W_j^3 \, d\Omega \qquad (42)$$

The "mass" matrices $\mathbf{M}$ and the "stiffness" matrices $\mathbf{S}$ are square and map l-forms to l-forms, the "derivative" matrices $\mathbf{D}$ are rectangular and map l-forms to $(l+1)$-forms. It can be shown that

$$\mathbf{D}^{01} = \mathbf{M}^1 \mathbf{K}^{01} \tag{43}$$

$$\mathbf{S}^0 = \left(\mathbf{K}^{01}\right)^T \mathbf{M}^1 \mathbf{K}^{01} \tag{44}$$

$$\mathbf{D}^{12} = \mathbf{M}^2 \mathbf{K}^{12} \tag{45}$$

$$\mathbf{S}^1 = \left(\mathbf{K}^{12}\right)^T \mathbf{M}^2 \mathbf{K}^{12} \tag{46}$$

$$\mathbf{D}^{23} = \mathbf{M}^3 \mathbf{K}^{23} \tag{47}$$

$$\mathbf{S}^2 = \left(\mathbf{K}^{23}\right)^T \mathbf{M}^3 \mathbf{K}^{23} \tag{48}$$

where $\mathbf{K}^{l(l+1)}$ is a "topological derivative" matrix. This matrix is the discretization of the exterior derivative operator d from differential geometry, $dW^l = W^{(l+1)}$. This matrix depends upon the mesh connectivity, but is independent of the nodal coordinates. It does not involve an integral over the element, and it does not involve any material properties. While seemingly abstract, it is enormously valuable in practice. The FEMSTER library computes the topological derivative matrices $\mathbf{K}^{01}$, $\mathbf{K}^{12}$, and $\mathbf{K}^{23}$. Given an l-form quantity X with basis function expansion

$$X = \sum_{i=1}^{n} x_i W_i^l, \tag{49}$$

and an $(l+1)$-form quantity Y with basis function expansion

$$Y = \sum_{i=1}^{n} y_i W_i^{(l+1)}, \tag{50}$$

the exterior derivative (gradient, curl, divergence for $l=0$, $l=1$, and $l=2$, respectively) is given by

$$\mathbf{y} = \mathbf{K}^{l(l+1)} \mathbf{x}. \tag{51}$$

It can be shown that

$$\mathbf{K}^{12}\mathbf{K}^{01} = 0 \tag{52}$$

$$\mathbf{K}^{23}\mathbf{K}^{12} = 0 \tag{53}$$

which are the discrete versions of $d(dW^l) = 0$. In terms of standard vector calculus, these matrix relations correspond to the identities $\vec{\nabla} \times \vec{\nabla} f = 0$ and $\vec{\nabla} \cdot \vec{\nabla} \times \vec{F} = 0$, respectively. These identities are satisfied in the discrete sense, exactly (to machine precision), for any mesh and any order basis function.

FEMSTER contains some additional miscellaneous functionality. In some circumstances it is necessary to convert an l-form to a $(3-l)-$form, i.e. a Hodge-star operation. A classic example is converting a "cell-center" quantity to a "nodal" quantity. In our finite element setting the Galerkin procedure prescribes rectangular matrices of the form

$$\mathbf{H}_{ij}^{p(3-l)} = \int_\Omega W_i^l \wedge W_j^{(3-l)} \, d\Omega \tag{54}$$

which produces optimal (in the least-square error sense) Hodge-star operators for arbitrary order basis functions. FEMSTER

also computes a variety of "load vectors" that are used as source terms in finite element discretizations,

$$\mathbf{f}_j^0 = \int_\Omega f \, W_j^0 \, d\Omega \tag{55}$$

$$\mathbf{f}_j^1 = \int_\Omega f \cdot W_j^1 \, d\Omega \tag{56}$$

$$\mathbf{f}_j^2 = \int_\Omega f \cdot W_j^2 \, d\Omega \tag{57}$$

$$\mathbf{f}_j^3 = \int_\Omega f \cdot W_j^3 \, d\Omega \tag{58}$$

$$\mathbf{g}_j^0 = \int_\Gamma g \, W_j^0 \, d\Gamma \tag{59}$$

$$\mathbf{g}_j^1 = \int_\Gamma g \cdot W_j^1 \, d\Gamma \tag{60}$$

$$\mathbf{g}_j^2 = \int_\Gamma g \cdot W_j^2 \, d\Gamma \tag{61}$$

C. Semi-Discrete $\vec{E}$ Field Formulation

Given the above defined matrices, the semi-discrete electric field formulation is given by the equations

$$\mathbf{M}^1(\sigma) \frac{\partial \mathbf{e}}{\partial t} = -\mathbf{S}^1(\mu^{-1}) \, \mathbf{e} - \mathbf{f}^1 \tag{62}$$

$$\frac{\partial \mathbf{b}}{\partial t} = -\mathbf{K}^{12} \, \mathbf{e} \tag{63}$$

$$\mathbf{M}^2(\sigma^{-1}) \, \mathbf{j} = \mathbf{H}^{12} \, \mathbf{e} \tag{64}$$

The divergence constraints are given by

$$\left(\mathbf{D}^{01}(\sigma)\right)^T \mathbf{e} = 0 \tag{65}$$

$$\mathbf{K}^{23}\mathbf{b} = 0 \tag{66}$$

and from the identities (52) and (53) these constraints are implicitly satisfied for all time, assuming the initial conditions and the source terms are divergence free. Hence in practice the divergence matrices are not constructed.

D. Semi-Discrete $\vec{H}$ Field Formulation

Given the above defined matrices, the semi-discrete magnetic field formulation is given by the equations

$$\mathbf{M}^1(\mu) \frac{\partial \mathbf{h}}{\partial t} = -\mathbf{S}^1(\sigma^{-1}) \, \mathbf{h} + (\mathbf{D}^{12}(\sigma^{-1}))^T \, \mathbf{f}^2 \tag{67}$$

$$\mathbf{M}^2(\mu^{-1}) \, \mathbf{b} = \mathbf{H}^{12} \, \mathbf{h} \tag{68}$$

$$\mathbf{j} = \mathbf{K}^{12} \, \mathbf{h} - \mathbf{f}^2 \tag{69}$$

The divergence constraints are given by

$$\left(\mathbf{D}^{01}(\mu)\right)^T \mathbf{h} = 0 \tag{70}$$

$$\mathbf{K}^{23}\mathbf{j} = 0 \tag{71}$$

and from the identities (52) and (53) these constraints are implicitly satisfied for all time, assuming the initial conditions and the source terms are divergence free.

E. Semi-Discrete $\vec{A}$-φ Potential Formulation

Given the above defined matrices, the semi-discrete magnetic vector potential formulation is given by the equations

$$\mathbf{S}^0(\sigma)\,\mathbf{v} \;=\; \mathbf{g}^0 \tag{72}$$

$$\mathbf{M}^1(\sigma)\,\frac{\partial \mathbf{a}}{\partial t} \;=\; -\mathbf{S}^1(\mu^{-1})\,\mathbf{a} - \mathbf{D}^{01}(\sigma)\,\mathbf{v} + \mathbf{f}^1 \tag{73}$$

$$\mathbf{e} \;=\; -\mathbf{K}^{01}\,\mathbf{v} - \frac{\partial \mathbf{a}}{\partial t} \tag{74}$$

$$\mathbf{b} \;=\; \mathbf{K}^{12}\,\mathbf{a} \tag{75}$$

$$\mathbf{M}^2(\sigma^{-1})\,\mathbf{j} \;=\; \mathbf{H}^{12}\,\mathbf{e} \tag{76}$$

The divergence constraints are given by

$$\left(\mathbf{D}^{01}(\sigma)\right)^T \mathbf{a} \;=\; 0 \tag{77}$$

$$\left(\mathbf{D}^{01}(\sigma)\right)^T \mathbf{e} \;=\; 0 \tag{78}$$

$$\mathbf{K}^{23}\mathbf{b} \;=\; 0 \tag{79}$$

and from the identities (52) and (53) these constraints are implicitly satisfied for all time, assuming the initial conditions and the source terms are divergence free.

IV. TIME INTEGRATION

The time integration scheme will be a generalized Crank-Nicholson method. This can be derived by averaging a first-order forward difference at time n with a first-order backward difference at time $n+1$. The averaging is performed with a weighting parameter α, where $0 \le \alpha \le 1$, such that

$$\alpha = \begin{cases} 0 & \text{Explicit, 1st Order Accurate Forward Euler} \\ 1/2 & \text{Implicit, 2nd Order Accurate Crank Nicholson} \\ 1 & \text{Implicit, 1st Order Accurate Backward Euler} \end{cases}$$

The method is unconditionally stable for $\alpha \ge 1/2$. For $\alpha < 1/2$, the stability condition is

$$\Delta t < \chi\left(\mathbf{M}^1(\sigma)^{-1}\mathbf{S}^1(\mu)\right), \tag{80}$$

where $\chi(Z)$ denotes the spectral radius of the matrix Z. This can be computed quite efficiently by the power method (see for example [29]) . Or, it can be estimated using the rule that $\Delta t < \kappa h^2$ where $\kappa = \frac{1}{\sigma \mu}$ is the magnetic diffusivity and h is the minimal mesh spacing.

A. Fully-Discrete $\vec{E}$ Field Formulation

For the electric field diffusion equation we have

$$\begin{aligned} \left(\mathbf{M}^1(\sigma) \;+\; \alpha\Delta t\mathbf{S}^1(\mu^{-1})\right)\mathbf{e}_{n+1} \\ =\; \left(\mathbf{M}^1(\sigma) - (1-\alpha)\Delta t\mathbf{S}^1(\mu^{-1})\right)\mathbf{e}_n \\ -\; \Delta t\mathbf{f}^1_{n+\alpha} \end{aligned} \tag{81}$$

$$\mathbf{b}_{n+1} \;=\; \mathbf{b}_n - \frac{\Delta t}{2}\mathbf{K}^{12}\left(\mathbf{e}_{n+1} + \mathbf{e}_n\right) \tag{82}$$

$$\mathbf{M}^2(\sigma^{-1})\mathbf{j}_{n+1} \;=\; \mathbf{H}^{12}\mathbf{e}_{n+1} \tag{83}$$

Note that the source function is evaluated at the intermediate time step $n+\alpha$.

B. Fully-Discrete $\vec{H}$ Field Formulation

The time integration for the magnetic diffusion equation is quite similar,

$$\begin{aligned} \left(\mathbf{M}^1(\mu) \;+\; \alpha\Delta t\mathbf{S}^1(\sigma^{-1})\right)\mathbf{h}_{n+1} \\ =\; \left(\mathbf{M}^1(\mu) - (1-\alpha)\Delta t\mathbf{S}^1(\sigma^{-1})\right)\mathbf{h}_n \\ +\; \Delta t(D^{12}(\sigma^{-1}))^T\,\mathbf{f}^2_{n+\alpha} \end{aligned} \tag{84}$$

$$\mathbf{M}^2(\mu^{-1})\,\mathbf{b}_{n+1} \;=\; \mathbf{H}^{12}\,\mathbf{h}_{n+1} \tag{85}$$

$$\mathbf{j}_{n+1} \;=\; \mathbf{K}^{12}\,\mathbf{h}_{n+1} - \mathbf{f}^2_{n+\alpha} \tag{86}$$

C. Fully-Discrete $\vec{A}$-φ Potential Formulation

The time integration for the potential diffusion equation is also quite similar,

$$\mathbf{S}^0\mathbf{v}_{n+\alpha} \;=\; \mathbf{f}^0_{n+\alpha} \tag{87}$$

$$\begin{aligned} \left(\mathbf{M}^1(\sigma) \;+\; \alpha\Delta t\mathbf{S}^1(\mu^{-1})\right)\mathbf{a}_{n+1} \\ =\; \left(\mathbf{M}^1(\sigma) - (1-\alpha)\Delta t\mathbf{S}^1(\mu^{-1})\right)\mathbf{a}_n \\ -\; \Delta t\mathbf{D}^{01}\mathbf{v}_{n+\alpha} + \mathbf{f}^1_{n+\alpha} \end{aligned} \tag{88}$$

$$\mathbf{e}_{n+\alpha} \;=\; -\mathbf{K}^{01}\mathbf{v}_{n+\alpha} - 1/\Delta t\left(\mathbf{a}_{n+1} - \mathbf{a}_n\right) \tag{89}$$

$$\mathbf{b}_{n+1} \;=\; \mathbf{K}^{12}\mathbf{a}_{n+1} \tag{90}$$

$$\mathbf{M}^2(\sigma^{-1})\mathbf{j}_{n+\alpha} \;=\; \mathbf{H}^{12}\mathbf{e}_{n+\alpha} \tag{91}$$

For this case, note that the discrete eddy current flux density $\mathbf{j}$ is known at intermediate time steps to maintain second order accuracy in time.

V. NUMERICAL EXPERIMENTS AND COMPUTATIONAL RESULTS

We now present a series of numerical experiments for the purposes of verifying the fully discrete equations of Section IV according to the criterion listed in Section I and [21]. Having analytic solutions to the continuum diffusion equations of Section II permits a normed error analysis, allowing us to verify the orders of accuracy for the proposed spatial and temporal discretization schemes. Analytic solutions to 3D PDE's are usually only available for problems with a high degree of spatial symmetry or for problems on certain canonical geometries such as cubes, cylinders and spheres. As such, we introduce three canonical problems in the calculation of transient eddy currents. For each canonical problem, we perform a convergence study in which we compute normed error quantities on a sequence of recursively refined meshes (h-refinement) and varying degrees of approximation for the finite element basis functions (p-refinement). In addition, we investigate the effect of element geometry on the error convergence properties of the methods by utilizing both standard orthogonal (Cartesian) meshes and more distorted varieties which have non-orthogonal elements with possibly non-coplanar quadrilateral faces. We also use a method of manufactured solutions specifically designed to verify the convergence properties of each of the methods.

Suppose $\vec{u}$ is a time dependent vector field which is an analytic solution to one of the continuum electromagnetic diffusion equations of Section II. We compute the error in the finite

element solution $\vec{u}_h$ of the corresponding discrete equation of Section IV at time step n using the $L2$ norm, defined as

$$\|\vec{u} - \vec{u}_h\|_2 \equiv \sqrt{\sum_k \left[\int_{\Omega_k} (\vec{u} - \vec{u}_h) \cdot (\vec{u} - \vec{u}_h) \, d\Omega_k \right]} \qquad (92)$$

Numerous analyses of the Galerkin finite element procedure using $H(Curl)$ basis functions for *curl-curl* equations indicate a theoretical convergence of

$$\|\vec{u} - \vec{u}_h\|_{H(curl)} \propto O(h^p), \qquad (93)$$

where p is the degree of the polynomial basis function and

$$\|\vec{u} - \vec{u}_h\|_{H(curl)} = \|\vec{u} - \vec{u}_h\|_2 + \left\| (\vec{\nabla} \times \vec{u}) - (\vec{\nabla} \times \vec{u}_h) \right\|_2. \qquad (94)$$

This is of course for problems with suitable regularity, we are not concerned here with problems in which the exact solution possess singularities. In the following examples, we use the $L2$ norm as this quantity is analogous to the root-mean-square error commonly applied in multifarious engineering disciplines. Since the $H(Curl)$ basis functions are incomplete, convergence in the $L2$ norm may be $O(h^p)$ or $O(h^{p+1})$ depending upon the specific problem, and misleading convergence results have been reported due to this phenomena. The examples below exemplify this. It must be noted that in this paper we refer to the lowest order $H(Curl)$ and $H(Div)$ basis functions as $p = 1$, even though these basis functions are incomplete.

In each of the following examples, a linear system involving finite element mass and stiffness matrices must be solved at every time step (by virtue of the implicit time integration method used). For each of the following examples, the linear systems are solved to a residual error tolerance of 10^{-10} using a diagonally scaled pre-conditioned conjugate gradient (PCG) iterative solver.

A. The "Wine Cellar" Problem – Cubic Geometry

This particular problem illustrates super-convergence of the numerical solution. Consider a simple 1D analytic solution to the scalar diffusion equation. This particular problem is sometimes referred to as the "wine cellar" problem as it can be used to determine the best depth of a cellar buried below ground level to minimize the variation in temperature due to the periodic changes in heat at ground level due to thermal radiation from the sun. The 1D diffusion equation is of the form

$$\frac{d}{dt} u(x,t) = \kappa \frac{d^2}{dx^2} u(x,t),$$

where the term κ is the thermal diffusivity. Suppose we impose the boundary conditions $u(0,t) = cos(\omega t)$ and $u(L,t) = 0$ for some fixed distance L and angular frequency ω, then a solution to this is given by

$$u(x,t) = \frac{\sin(\beta x)}{\sin(\beta L)} \exp(-i\omega t), \qquad (95)$$

where $\beta = \frac{\sqrt{i\omega}}{\kappa}$ (here i denotes $\sqrt{-1}$). We can adapt this simple 1D problem to a three dimensional vector field problem by considering a cubic domain of width, length and height equal to L. Consider an electric field vector of the form

$$\vec{E} = u(z,t) \, \hat{x}, \qquad (96)$$

i.e. the electric field is oriented with respect to the positive x-axis of the cubic domain and diffuses in the z-direction. The electric field of (96) is a solution to (6) with $\kappa = \frac{1}{\sqrt{\mu\sigma}}$, $\vec{J}_s = 0$ (i.e. no external current source), and subject to the Dirichlet boundary conditions: $\hat{n} \times \vec{E} = u(0,t)$ at the $z = 0$ face and $\hat{n} \times \vec{E} = 0$ at the $z = L, x = 0$ and $x = L$ faces. The remaining two faces of the cubic domain satisfy the natural boundary condition of (10).

We now perform a normed error analysis of the computed solution. We performed a total of 12 computational experiments: a sequence of 3 orthogonal Cartesian meshes, a sequence of 3 skewed non-orthogonal meshes, and both $p = 1$ and $p = 2$ basis functions for each mesh. A value of $\alpha = 0.5$ was used for the time stepping for 2nd order accuracy. For every level of refinement (in h or p), the time step Δt was refined as well, so that time integration error would not dominate. An example of the $\vec{E}$ and $\vec{B}$ fields, computed using the $\vec{E}$ field formulation, is shown in Figure 1, and the computed $\vec{E}$ field is compared to the exact solution in Figure 2. An example of the computed error distribution, for both the Cartesian and the skewed mesh, is shown in Figure 3. Clearly, for the skewed mesh, the error is concentrated in the vicinity of the most distorted elements. In Table II we list the computational statistics for the experiments including the total number of Degrees of Freedom (DoF) for each experiment. Note that the average number of PCG iterations required to achieve the same error tolerance increases for the case of the skewed mesh as expected.

The convergence for the 12 computations is shown in Figure 4. Note that for the Cartesian mesh the $L2$ error converges at a rate of $O(h^{p+1})$, whereas for the skewed mesh the $L2$ error converges at a rate of $O(h^p)$. The Cartesian case exhibits super-convergence. This is not a general result - it is due to the fact that for this specific problem the electric field $\vec{E} = E_x \hat{x}$ is aligned with the mesh edges, and E_x is independent of x. The example in Section V-D shows that the generic convergence is $O(h^p)$ even for orthogonal Cartesian meshes. The computed convergence for the skewed meshes agrees with the theoretical expectation. It should be noted that the $\vec{H}$ field formulation and the $\vec{A}$ field formulation give identical rates of convergence for this problem.

B. The "Conducting Pipe" Problem – Cylindrical Geometry

Consider a conducting pipe of conductivity σ with inner radius R_i, outer radius R_o and total length L oriented along the $\hat{z}$-axis. Suppose there is a time harmonic current source $f(\omega t)$ on the $\hat{z}$-axis, generating a magnetic field intensity of the form $\vec{H} = \frac{f(\omega t)}{2\pi r} \hat{\theta}$. Analytic solutions for the time dependent magnetic field intensity $\vec{H}$ and transient eddy current density $\vec{J}$ inside of the conducting pipe exist and can be expressed in terms of modified Bessel functions of the first kind, $I_n(z)$, and the second kind, $K_n(z)$. The exact magnetic field intensity is of the form

$$\vec{H}(r,t) = (c_0 I_1(\alpha r) + c_1 K_1(\alpha r)) \exp(i\omega t) \hat{\theta}, \qquad (97)$$
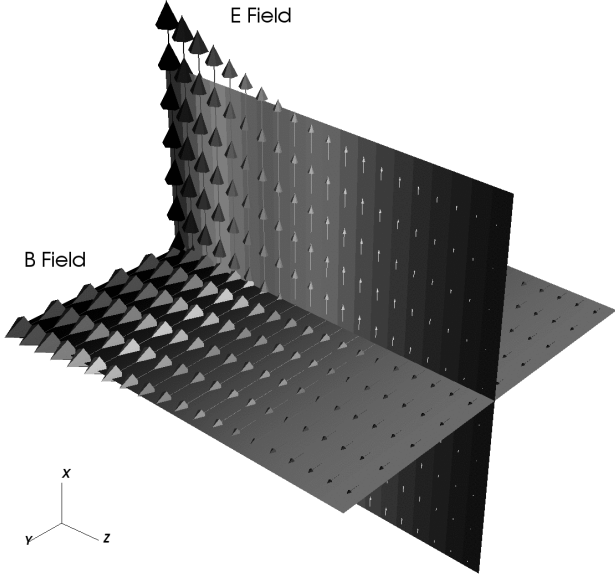
Fig. 1. Electric and magnetic fields in the wine cellar problem at a snapshot in time computed using the fully discrete $\vec{E}$ field formulation on the $h2$ Cartesian mesh.
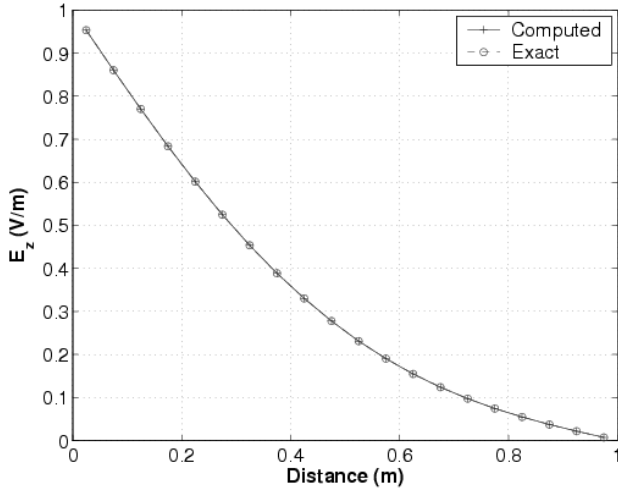

Fig. 2. Comparison of computed $\hat{x}$-component of electric field to exact analytic value at a snapshot in time on the $h2$ Cartesian mesh.

	No. Elems.	No. DoF	PCG Iterations (Cart / Skew)
h1-p1	1,000	3,630	10 / 30
h2-p1	8,000	26,460	16 / 35
h3-p1	64,000	201,720	16 / 39
h1-p2	1,000	26,460	18 / 45
h2-p2	8,000	201,720	18 / 51
h3-p2	64,000	1,574,640	19 / 55

TABLE II

RESULTS FOR hp-REFINED FINITE ELEMENT SOLUTIONS TO THE WINE CELLAR PROBLEM USING THE FULLY DISCRETE $\vec{E}$ FIELD FORMULATION.
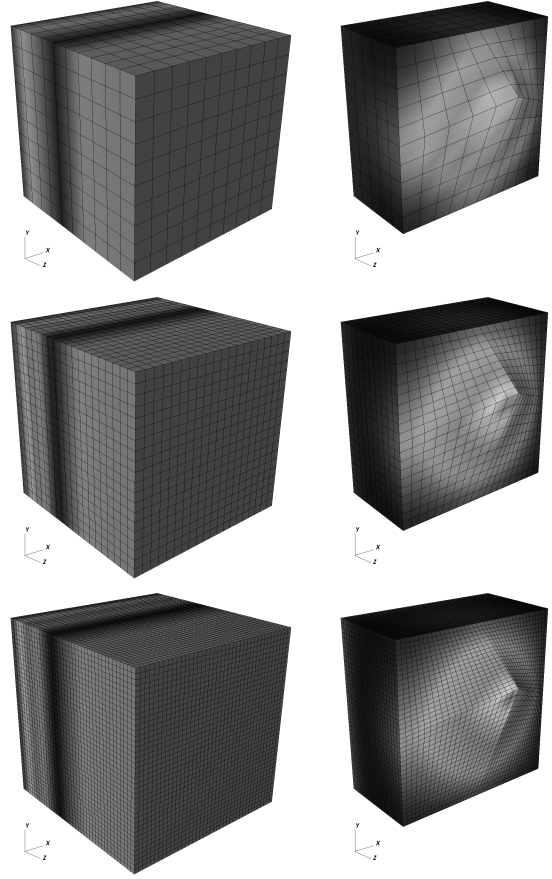
Fig. 3. Cartesian (*left*) and skewed (*right*) wine cellar meshes with pseudo-color plot of error distribution.

while the exact eddy currents are of the form

$$\vec{J}(r,t) = \alpha(c_0 I_0(\alpha r) - c_1 K_0(\alpha r)) \exp(i\omega t)\hat{z}, \qquad (98)$$

where the coefficients are given by

$$\alpha = \frac{i+1}{\sqrt{2/(\omega\sigma\mu)}},$$

$$c_0 = \frac{R_i K_1(\alpha R_i) - R_o K_1(\alpha R_o)}{2\pi R_i R_o \left(I_1(\alpha R_o)K_1(\alpha R_i) - I_1(\alpha R_i)K_1(\alpha R_o)\right)},$$

$$c_1 = \frac{-R_i I_1(\alpha R_i) + R_o I_1(\alpha R_o)}{2\pi R_i R_o \left(I_1(\alpha R_o)K_1(\alpha R_i) - I_1(\alpha R_i)K_1(\alpha R_o)\right)},$$

We now use (97) and (98) to perform a normed error analysis for the fully discrete magnetic field diffusion equations of (84) and (86) using a sequence of refined cylindrical meshes (*h*-refinement) and varying degrees of approximation for the finite element basis functions (*p*-refinement). To fully define the problem, we apply a time dependent Dirichlet boundary condition $\hat{n} \times \vec{H} = \vec{H}(R_i, t)$ to the inner cylindrical surface defined by $r = R_i$, and $\hat{n} \times \vec{H} = \vec{H}(R_o, t)$ to the outer cylindrical surface defined by $r = R_o$. The top and bottom faces of the cylinder (defined by the surfaces $z = 0$ and $z = L$) satisfy the natural boundary condition of (17). We performed 36 experiments: a sequence of 3 orthogonal cylindrical meshes, a sequence of 3 skewed cylindrical meshes, and $p = 1, 2, 3$ basis functions for
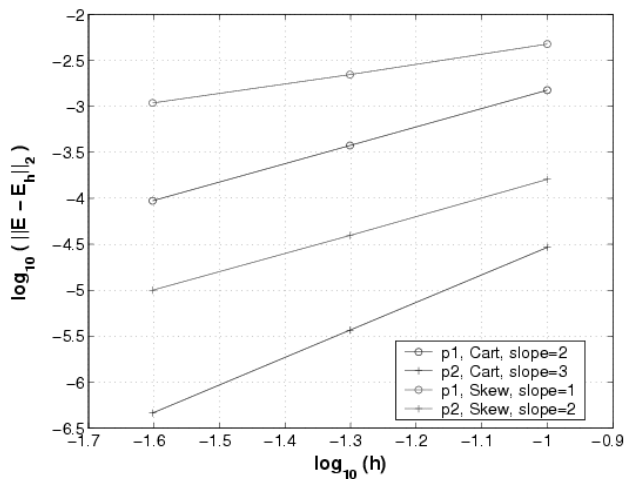
Fig. 4. Convergence of wine cellar solution using the fully discrete $\vec{E}$ field formulation.

Fig. 5. Magnetic and eddy current fields in conducting pipe problem at a snapshot in time computed using the fully discrete $\vec{H}$ field formulation on the $h2$ orthogonal mesh.

each mesh. A snapshot of the computed fields is shown in Figure 5, and comparisons of the computed fields and currents to the exact fields and currents are shown in Figure 6 and Figure 7 respectively, again at one snapshot in time. The computed $L2$ error distribution is shown for the 6 different meshes, again at one snapshot in time Figure 8. In Table III we list the computational statistics for the experiments. Again, note that the average number of PCG iterations required to achieve the same error tolerance increases for the case of the skewed mesh as expected.

The rates of convergence for the conducting pipe problem, for the magnetic field and for the the eddy current density, are shown in Figure 9 and Figure 10, respectively. Examining Figure 9 we see the rate of convergence for the orthogonal mesh is $O(h^2)$ for $p = 1$, $O(h^2)$ for $p = 2$, and $O(h^4)$ for $p = 3$. We see super-convergence for odd degree basis functions. The reason for super convergence is again due to the fact that the mesh edges are aligned with the $\vec{H}$ field. No super-convergence is seen for the skewed mesh. The super-convergence for odd degree basis functions is because the Bessel functions $I_1(z)$ and $K_1(z)$ have Taylor series expansions that involve only odd powers of z, increasing the degree of the basis function from $p = 2$ to $p = 3$ annihilates another term in the Taylor series expansion. Examining the rates of convergence for the eddy current density shows no super-convergence, this is due to the fact that the Taylor series expansion for the eddy current involves $Log(z)$ terms.

C. Transients in a Conducting Sphere – Spherical Geometry

In this example, rather than driving the problem with a time-harmonic boundary condition, we have an initial magnetic field that decays away with time. We also use an unstructured mesh to demonstrate that this does not degrade the performance of the finite element method. Consider a conducting sphere of radius a, conductivity σ and permeability μ placed in an external alternating magnetic field with amplitude B and angular frequency ω. At time $t = 0$, the magnetic field is switched off and we observe what happens to the vector potential in the sphere as a function of time. The exact analytic solution to this problem is
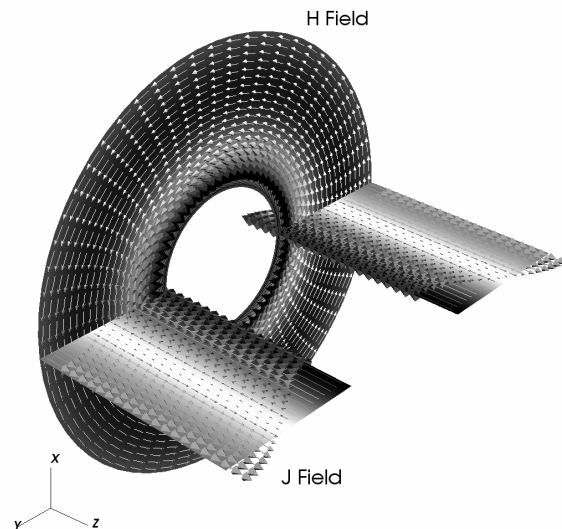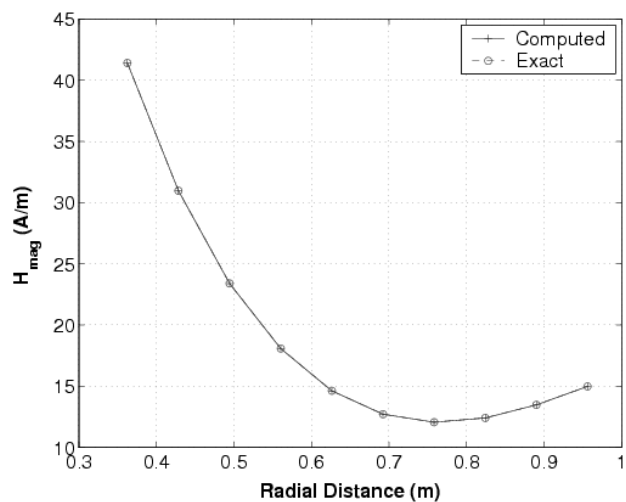

Fig. 6. Comparison of computed magnitude of magnetic field intensity to exact analytic value at a snapshot in time on the $h2$ orthogonal mesh.

a sum of Bessel functions and requires the solution of a transcendental equation to obtain the series coefficients of the sum as described in [23]

$$\vec{A} = \begin{cases} \sum_s \mathcal{A}_s r^{-\frac{1}{2}} J_{\frac{3}{2}}(k_s r) \sin(\theta) \exp\left(-\frac{k_s^2 t}{\sigma \mu}\right) \hat{\phi} & r \leq a \\ \sum_s \mathcal{B}_s r^{-2} \sin(\theta) \exp\left(-\frac{k_s^2 t}{\sigma \mu}\right) \hat{\phi} & r > a \end{cases} \quad (99)$$

The expansion coefficients are computed as

$$\mathcal{A}_s = \frac{3\frac{\mu}{\mu_0} B a^{\frac{3}{2}}}{\left(k_s^2 a^2 (\frac{\mu}{\mu_0} + 2)(\frac{\mu}{\mu_0} - 1)\right) J_{\frac{3}{2}}(k_s a)}$$

$$\mathcal{B}_s = \mathcal{A}_s a^{\frac{3}{2}} J_{\frac{3}{2}}(k_s a)$$
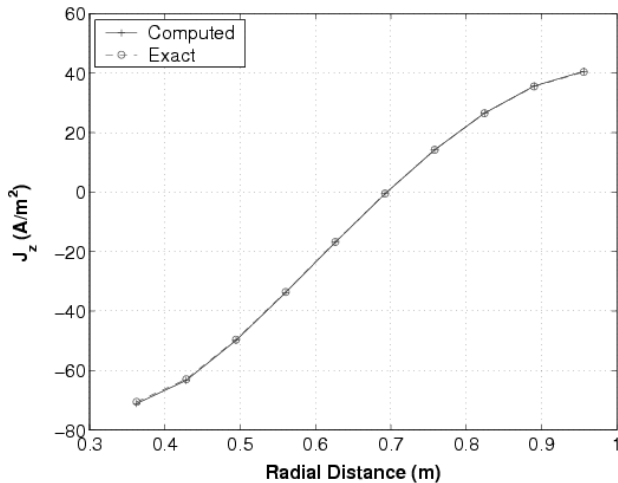
Fig. 7. Comparison of computed $\hat{z}$-component of eddy current to exact analytic value at a snapshot in time on the $h2$ orthogonal mesh.

	No. Elems.	No. DoF	PCG Iterations (Orth / Skew)
h1-p1	375	1,440	6 / 12
h2-p1	3,000	10,230	10 / 21
h3-p1	24,000	76,860	16 / 29
h1-p2	375	10,230	16 / 51
h2-p2	3,000	76,860	18 / 55
h3-p2	24,000	595,320	18 / 60
h1-p3	375	33,120	23 / 58
h2-p3	3,000	253,890	22 / 58
h3-p3	24,000	1,686,828	21 / 59

TABLE III

RESULTS FOR hp-REFINED FINITE ELEMENT SOLUTIONS TO THE CONDUCTING PIPE PROBLEM USING THE FULLY DISCRETE $\vec{H}$ FIELD FORMULATION.

The coefficients k_s must be computed by solving the transcendental equation

$$\mu_0 a \frac{d}{dr}[J_{\frac{3}{2}}(k_s r)]|_{r=a} + (\mu + \frac{1}{2}\mu_0)J_{\frac{3}{2}}(k_s a) = 0$$

In this example, we use the $\vec{A}$-ϕ potential formulation and the exact solution to perform $L2$ normed error analysis. We discretize the problem in space for two spherical meshes, a relatively coarse mesh with characteristic element volume $8\Delta h$ and a fine mesh with element volume Δh. The vector potential formulation is integrated in time via (88) for a total physical time of $20s$. For the coarse mesh, a time step of $\Delta t = 0.01s$ is used for total of 2000 time steps while for the fine mesh a time step of $\Delta t = 0.005s$ for a total of 4000 time steps. The exact solution of (99) is used as both an initial condition and a time dependent boundary condition in the FEM calculation. In Figure 11 we plot the computed vector potential inside the sphere after 100 time steps and compare this to the analytic result in Figure 12. In Figure 13 we plot the $L2$ error as a function of time for

Fig. 8. Orthogonal (*left*) and skewed (*right*) conducting pipe meshes with pseudo-color plot of error distribution.

the two spherical meshes. The error decreases with time, since the fields are decreasing in magnitude due to electromagnetic diffusion. While not shown here, the convergence for this particular problem was experimentally confirmed to be $O(h^p)$, no super-convergence was observed, as expected due to the use of an unstructured mesh.

D. Method of Manufactured Solution

In the previous computational experiments we begin with a geometry, we impose boundary conditions and initial conditions, and we proceed to compute the exact analytical solution to the problem. The method of manufactured solutions is a different approach. Here we begin with a functional form of the solution field which can be based on polynomials, trigonometric functions, etc. This solution field is then plugged into the PDE to determine the source terms and the boundary conditions. The goal is then to compare the computed finite element solution to the manufactured solution. In this example our goal is to demonstrate that each of the three fully-discrete field formulations of Section IV will yield the same convergence properties, even for the secondary quantities, the magnetic flux density $\vec{B}$ and the induced eddy current field $\vec{J}$.

Consider the following scalar and vector potentials

$$\phi = z \tag{100}$$

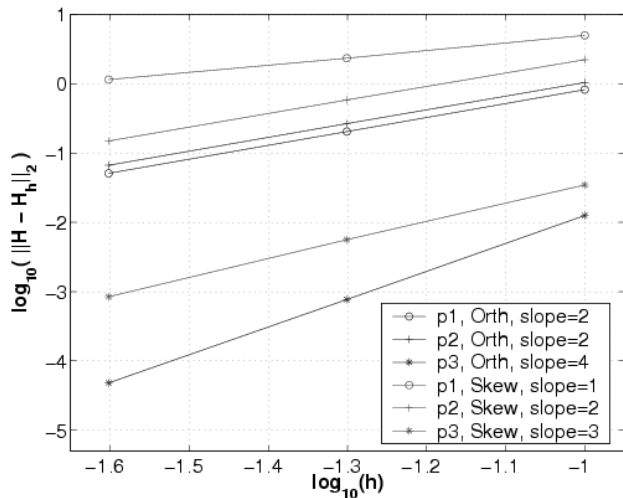$$\vec{A} = cos(\omega t + \frac{\pi}{4})\exp(x+y)(\hat{x}-\hat{y}) \tag{101}$$

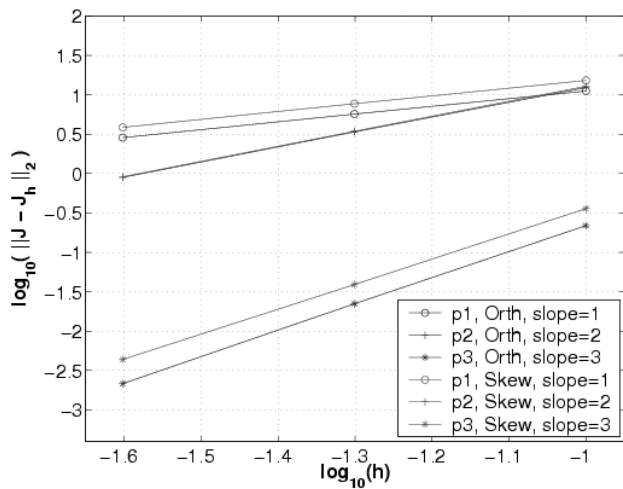Fig. 9. Convergence of conducting pipe magnetic field solution using the fully discrete $\vec{H}$ field formulation.

Fig. 10. Convergence of conducting pipe eddy current solution using the fully discrete $\vec{H}$ field formulation.

Fig. 11. Vector potential in the conducting sphere problem at a snapshot in time computed using the fully discrete $\vec{A}$-ϕ potential formulation.

Fig. 12. Comparison of computed magnitude of vector potential to exact analytic value at a snapshot in time on the fine spherical mesh.

Fig. 13. Computed $L2$ error vs. time for two spherical meshes.

Note that ϕ satisfies the Poisson equation of (20) and that $\vec{A}$ satisfies the gauge condition $\vec{\nabla} \cdot \sigma \vec{A} = 0$. In addition, we have chosen the vector potential $\vec{A}$ such that its $\hat{x}$ and $\hat{y}$ components are infinitely differentiable in x and y, and the Taylor series expansion contains all powers of x and y. We therefore expect $O(h^p)$ convergence. Given these two analytic fields, we can generate corresponding analytic values for the remaining primary field variables

$$\vec{E} = \omega sin(\omega t + \frac{\pi}{4}) \exp(x+y)(\hat{x} - \hat{y}) - \hat{z} \quad (102)$$

$$\vec{H} = -\frac{2}{\mu} \exp(x+y) \cos(\omega t + \frac{\pi}{4})\hat{z} \quad (103)$$

We are interested in the convergence properties of the secondary variables, and for the values chosen in (100) and (101), they are given by

$$\vec{B} = -2 \exp(x+y) \cos(\omega t + \frac{\pi}{4})\hat{z} \quad (104)$$

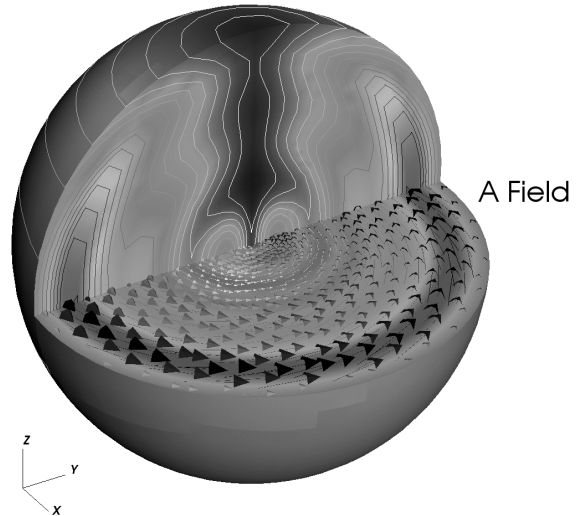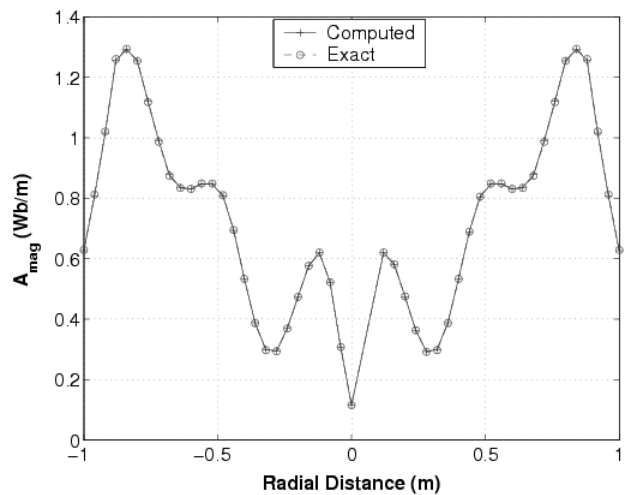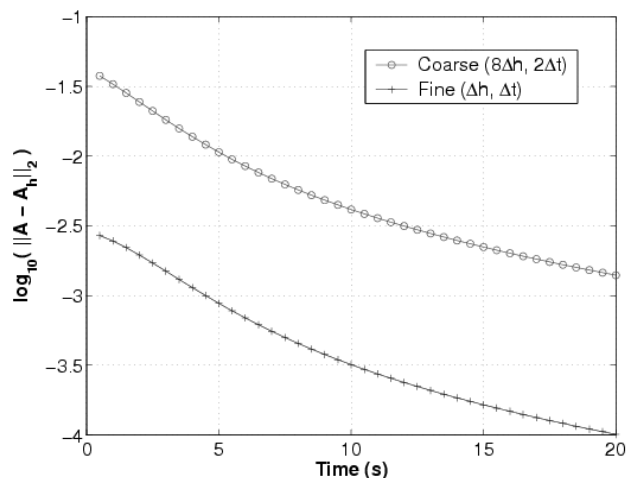$$\vec{J} = \sigma \omega sin(\omega t + \frac{\pi}{4}) \exp(x+y)(\hat{x} - \hat{y}) - \sigma \hat{z} \quad (105)$$

Finally, the corresponding independent current source term that will drive the problem is given by

$$\vec{J}_s = \exp(x+y)\left(\frac{2}{\mu}\cos\left(\omega t + \frac{\pi}{4}\right) + \sigma\omega\sin\left(\omega t + \frac{\pi}{4}\right)\right)(\hat{y}-\hat{x}) + \sigma\hat{z}$$

Note that a phase shift of $\frac{\pi}{4}$ has been added to the time dependence of each term to ensure that each of the primary fields $\vec{A}, \vec{E}$ and $\vec{H}$ will have a non-zero value at time $t = 0$.

The problem domain Ω is a simple unit cube of conductivity $\sigma = 10^7 \, S \, m^{-1}$ and permeability $\mu = 4\pi \, 10^{-7} \, Wb \, A^{-1} \, m^{-1}$. Fixing the skin depth of the cube to be 0.5 yields an angular frequency $\omega = 0.63662 Hz$. We run each of the following test problems for a total physical time of $0.02s$. We use the analytic value of the primary field variables as the time dependent Dirichlet boundary condition, as well as for the initial condition for each of the fully discrete formulations of Section IV.

To compute the error convergence in the computation of $\vec{B}$ and $\vec{J}$ using each of the fully discrete formulations, we begin with a base-line coarse model consisting of 1,000 Cartesian hexahedral elements. We choose a discrete time step $\Delta t = 10^{-4}s$ and run each of the three diffusion formulations for a total of 200 time steps using low order $p = 1$ basis functions. At the final time step, we extract the global $L2$ error for the computed magnetic flux density and eddy current density. We repeat this computation for 2 additional levels of h-Refinement and 1 additional level of p-Refinement for a total of 6 runs for each formulation. For each level of refinement (h or p), the discrete time step is cut in half and the total number of time steps is doubled. This is done to ensure that the spatial discretization will be the dominant source of error.

In Figure 14 we plot the $L2$ error of the magnetic flux density $||\vec{B} - \vec{B}_h||_2$ vs. the characteristic element size h on a log-log scale. In Figure 15 we plot the the $L2$ error of the eddy current density $||\vec{J} - \vec{J}_h||_2$. The slope of each line indicates the rate at which the error is converging. Note that for the case of low order $p = 1$ basis functions, all three formulations yield essentially the same error with a convergence rate of $O(h)$ in agreement with the predictions of theory. For the case of $p = 2$ basis functions, each formulation is converging at a rate of $O(h^2)$, again in agreement with the predictions of theory. The results for the eddy current density J are shown in Figure 15, with identical rates of convergence for each formulations.

While we refer to $\vec{B}$ and $\vec{J}$ as secondary quantities, they are often the quantity of interest if one is concerned with computing electromagnetic forces and stresses. These computational experiments show that the $\vec{E}$ field formulation, the $\vec{H}$ field formulation, and the $\vec{A}$-ϕ potential formulation give equally accurate results. There is no loss of accuracy in computing $\vec{B}$ from $\vec{B} = \vec{\nabla} \times \vec{A}$, or computing $\vec{J}$ from $\vec{J} = \vec{\nabla} \times \vec{H}$. Hence the choice of which formulation to use is really a matter of convenience, as each formulation has different Essential and Natural boundary conditions.

E. Electromagnetic Diffusion in Highly Heterogeneous Conducting Regions

Up until this point, we have ignored problems which contain regions of zero conductivity. Realistic eddy current problems
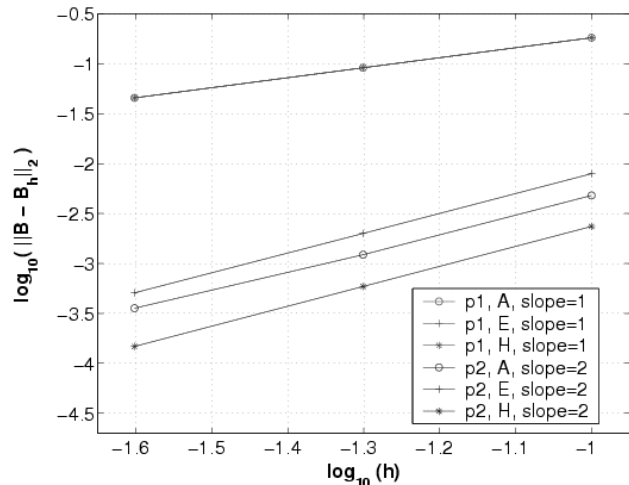

Fig. 14. Convergence of manufactured magnetic field solution using the three different formulations. Note that each method has the same rate of error convergence.
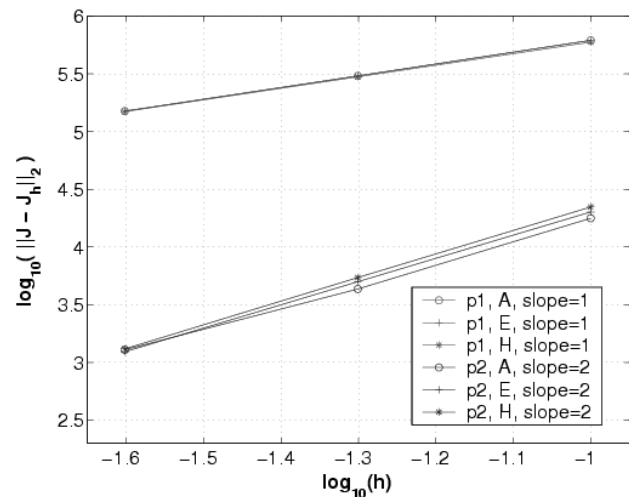

Fig. 15. Convergence of manufactured eddy current solution using the three different formulations. Note that each method has the same rate of error convergence.

involve configurations of conducting regions surrounded by a non-conducting medium (typically air). Simply setting $\sigma = 0$ in the diffusion formulations is not permitted as this results in an ill-defined problem. As mentioned in Section I, one way to overcome this problem is to simply assign a very small conductivity to the non-conducting regions to permit a numerical solution. This raises questions of numerical accuracy and linear solver performance. In this section, we investigate the numerical properties of electromagnetic diffusion in highly heterogeneous conducting regions. This particular numerical experiment is adapted from the first test problem in [3].

The problem region consists of a highly conductive ($\sigma = 63.3 \, 10^6 \, S \, m^{-1}$) "horse-shoe" with a region of air in between as depicted in Figure 16. The problem is driven by applying a constant tangential magnetic field value ($\hat{n} \times \vec{H}$) to the outer face of the air region. In order to numerically solve the problem, a conductivity of $\sigma = 1 \, S \, m^{-1}$ is assigned to the air region. In [3], the problem is discretized on a 2D mesh using a novel magnetic-
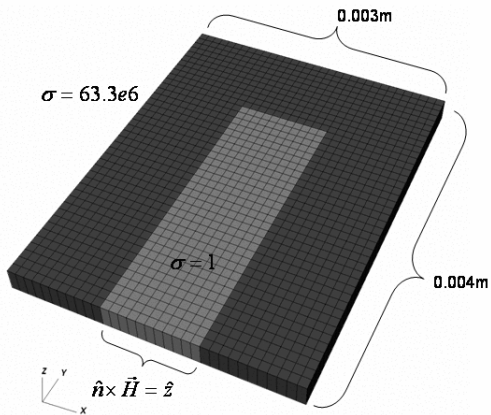
Fig. 16. Computational domain consisting of a conducting region and an air-like region of extremely low conductivity.

Fig. 18. Computed initial state (*left*) and final state (*right*) of $\vec{J}$ field using the fully discrete $\vec{H}$ field formulation.

conductivities. The first is convergence behavior of iterative solvers. In Table IV we list the solver performance statistics for 4 different experiments. Note that use of high order basis functions results in a drastic increase in the total number of iterations required to achieve convergence. It is interesting to note the difference in solver performance between the two formulations. The $\vec{H}$ field formulation results in a much better conditioned system due to the location of the material properties with respect to the mass and stiffness matrices. The second issue involves the time discretization. Because of the extremely fast diffusion times in the low-conductivity air regions, use of the second order accurate time integration option ($\alpha = 0.5$) can result in a "ringing" phenomenon as seen in Figure 19. This can be averted by using the fully implicit option ($\alpha = 1.0$) or by taking smaller time steps. Note that the $\vec{H}$ field formulation does not exhibit the "ringing" phenomenon even when using the second order accurate ($\alpha = 0.5$) option for this particular problem.

flux formulation and the resulting linear system is solved via a direct method. Here we solve the exact same problem using a 3D slab mesh (i.e. one element thick) using both the $\vec{A}$-ϕ potential formulation and the $\vec{H}$ field formulation (the constant $\vec{H}$ field boundary value precludes the use of the $\vec{E}$ field formulation) and an iterative solver for the resulting linear system.

For the $\vec{A}$-ϕ potential formulation, the $\hat{n} \times \vec{H}$ boundary condition is implemented via the inhomogeneous Neumann (or Natural) boundary condition $\hat{n} \times \frac{1}{\mu}\vec{\nabla} \times \vec{A}$ while for the $\vec{H}$ field formulation it is implemented via the Essential boundary condition. The problem is discretized in time using a time-step of $\Delta t = 2.5 \, 10^{-6} s$ for a total of 20 steps, enough time for the fields to reach steady state. A linear system is solved at every time step using a simple diagonally scaled PCG method with a residual tolerance of 10^{-8}. In both cases, the magnetic field effectively diffuses "instantly" after the first time step into the entire air-region due to the extremely low conductivity. Both formulations yield identical diffusion times for the $\vec{B}$ and $\vec{J}$ fields inside the conductor which are consistent with those reported in [3] (see Figure 17 and Figure 18).
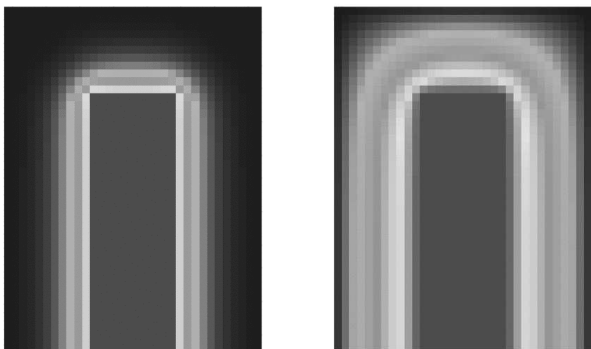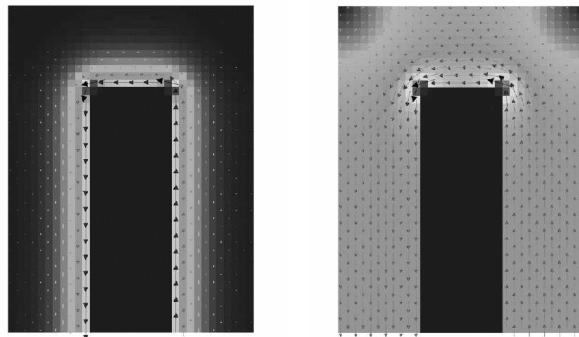
	No. DoF	Avg. PCG Iterations
A-p1	7,156	149
H-p1	7,156	51
A-p2	45,104	450
H-p2	45,104	145

TABLE IV

RESULTS FOR *p*-REFINED FINITE ELEMENT SOLUTIONS TO THE HETEROGENEOUS CONDUCTING REGION DIFFUSION TEST USING BOTH THE FULLY DISCRETE $\vec{A}$-ϕ POTENTIAL AND $\vec{H}$ FIELD FORMULATIONS.

Fig. 17. Computed initial state (*left*) and final state (*right*) of $\vec{B}$ field magnitude using the fully discrete $\vec{A}$-ϕ potential formulation.

VI. CONCLUSIONS

In this paper we review three different formulations for the time-dependent eddy current problem. These three formulations employ either the $\vec{E}$ field, the $\vec{H}$ field, or the $\vec{A}$ field as the primary field variable. For each formulation, we also show how secondary fields such as the magnetic flux density $\vec{B}$ and the eddy current density $\vec{J}$ can be computed. For each formulation the primary field variable is represented as a 1-form, and the secondary field variables are represented as 2-forms.

While this approach is suitable for most applications, there are numerical consequences of having such large variations in
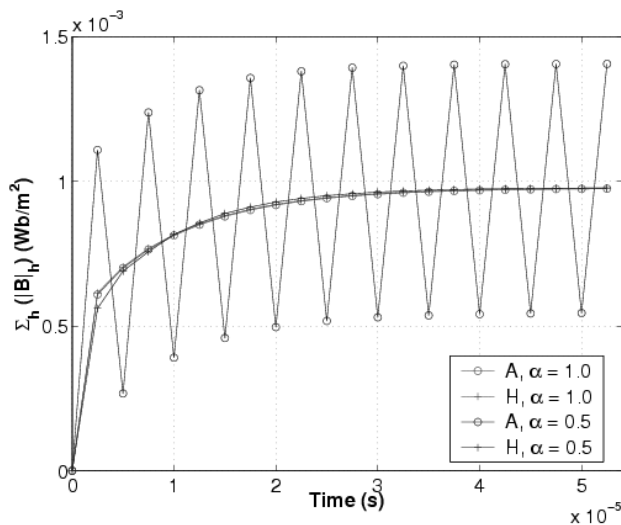
Fig. 19. Time history of the magnetic field using two different formulations with two different time integration options.

Each formulation involves a vector diffusion equation for the primary field variable, an additional curl equation, and an additional Hodge-star operation. The results of numerous computational experiments were presented, and anomalous super-convergence results were illustrated and explained. The key result is that these three formulations give equally accurate results, even for the secondary fields. If field $\vec{X}$ is computed with accuracy $O(h^p)$ in the L2 sense, then field $\vec{Y} = \vec{\nabla} \times \vec{X}$ is also computed with accuracy $O(h^p)$ in the L2 sense. In addition, it is demonstrated that the use of the Hodge-star operator does not degrade the accuracy either. Since each formulation utilizes essentially the same discrete operators, it is quite simple to implement all three formulations in a single code, and to use the formulation whose essential and/or natural boundary conditions best match the given problem.

REFERENCES

[1] Z. Ren, F. Bouillault, A. Razek, A. Bossavit, and J. C. Verite. A new hybrid model using electric field formulation for 3d eddy current problems. *IEEE Trans. Mag.*, 26(2):470–473, 1990.

[2] Z. Ren and A. Razek. A new technique for solving three-dimensional multiply connected eddy current problems. *IEE Proc.-A-Sci. Measure. Tech.*, 137(3):135–140, 1990.

[3] P. Bochev, J. Hu, A. Robinson, and R. Tuminaro. Towards robust Z-pinch simulations: Discretization and fast solvers for magnetic diffusion in heterogenous conductors. *Electronic Trans. Num. Analysis*, 15:186–210, 2003.

[4] A. Bossavit and J. C. Verite. The "TRIFOU" code: Solving the 3d eddy current problems by using H as the state variable. *IEEE Trans. Mag.*, 19(6):2465–2470, 1983.

[5] A. Bossavit. *Computational Electromagnetism: Variational Formulation, Complementarity, Edge Elements.* Academic Press, 1998.

[6] O. Biro and K. Preis. On the use of the magnetic vector potential in the finite element analysis of three-dimensional eddy currents. *IEEE Trans. Mag.*, 25(4):3145–3159, 1989.

[7] O. Biro, K. Preis, W Renhart, K. Richter, and G. Vrisk. Performance of different vector potential formulations in solving multiply connected eddy current problems. *IEEE Trans. Mag.*, 26(2):438–441, 1990.

[8] C. Bryant, C Emson, and C Trowbridge. A comparison of Lorentz gauge formulations in eddy current problems. *IEEE Trans. Mag.*, 26(2):430–433, 1990.

[9] B. Weis and O. Biro. Onthe convergence of transient eddy-curent problems. *IEEE Trans. Mag.*, 40(2):957–960, 2004.

[10] K. Fujiwara Y. Okada T. Nakata, N. Takahashi. Improvements in the $t - \omega$ method for eddy current analysis. *IEEE Trans. Mag.*, 24:94–97, 1988.

[11] H. Whitney. *Geometric Integration Theory*. Princeton University Press, 1957.

[12] J. C. Nédélec. Mixed finite elements in R3. *Numer. Math.*, 35:315–341, 1980.

[13] J. C. Nédélec. A new family of mixed finite elements in R3. *Numer. Math.*, 50:57–81, 1986.

[14] P.A. Raviart and J.M. Thomas. A Mixed Finite Element Method for 2nd Order Elliptic Problems. In I. Galligani and E. Mayera, editors, *Mathematical Aspects of the Finite Element Method*, volume 606 of *Lect. Notes. on Mathematics*, pages 293–315. Springer Verlag, 1977.

[15] J. Jin. *The Finite Element Method in Electromagnetics*. Wiley, 1993.

[16] M. Salazar-Palma, T. K. Sarkar, L. Garcia-Castillo, T. Roy, and A. Djordjevic. *Iterative and Self Adaptive Finite-Elements in Electromagnetic Modeling*. Artech House, 1998.

[17] P. Castillo, R. Rieben, and D. White. FEMSTER: An object oriented class library of discrete differential forms. In *Proceedings of the 2003 IEEE International Antennas and Propagation Symposium*, volume 2, pages 972–975, Columbus, Ohio, June 2003.

[18] M. Ainsworth. Dispersive properties of high-order Nedelec/edge element approximation of the time-harmonic Maxwell equations. *Philisophical Transactions of the Royal Society of London*, 362(1816):471–491, 2004.

[19] R. Rieben, D. White, and G. Rodrigue. A high order mixed vector finite element method for solving the time dependent Maxwell equations on unstructured grids. *J. Comput. Phys.*, 204:490–519, 2005.

[20] R. Rieben, D. White, and G. Rodrigue. High order symplectic integration methods for finite element solutions to time dependent maxwell equations. *IEEE Trans. Ant. Prop.*, 52(8):2190–2195, 2004.

[21] D. Post and L. Votta. Computational science demands a new paradigm. *Physics Today*, 58(1):35–41, January 2005.

[22] H. Ammari, A. Buffa, and J. C. Nedelec. A justification of eddy currents for the Maxwell equations. *SIAM J. Appl. Math.*, 60(5):1805–1823, 2000.

[23] W. R. Smythe. *Static and Dynamic Electricity*. McGraww-Hill, 1968.

[24] L. D. Landau and E. M. Lifshitz. *Electrodynaimcs of continuous media*. Peragom Press, 1960.

[25] H. E. Knoepfel. *Magnetic Fields*. Wiley, 2000.

[26] Andrzej Krawczyk and John A. Tegopoulos. *Numerical Modelling of Eddy Currents*. Oxford University / Clarendon Press, 1993.

[27] P. Castillo, J.Koining, R. Rieben, M. Stowell, and D. White. Discrete differential forms: A novel methodology for robust computational electromagnetics. Technical Report UCRL-ID-151522, Lawrence Livermore National Laboratory, Center for Applied Scientific Computing, January 2003.

[28] P. Castillo, R. Rieben, and D. White. FEMSTER: An object orienetd class library of higher-order discrete differential forms. *ACM Trans. Math. Soft.* in press.

[29] R. L. Burden and J. D. Faires. *Numerical Analysis*. Brooks/Cole Publishing, 6th edition, 1997.

Robert N. Rieben (M'03) received his B.S. in physics from the University of California at Riverside in 1999 and his Ph.D. in engineering / applied science from the Department of Applied Science, University of California at Davis. He is currently a post-doctoral researcher with the Defense Sciences Engineering Division at the Lawrence Livermore National Laboratory. His research interests include massively parallel physics simulations using high order numerical methods, time-domain vector finite element methods, the modeling and simulation of electromagnetic wave propagation, transient eddy current phenomena, photonic crystals and photonic band-gap structures and magnetohydrodynamics.

Daniel A. White (M'88) received the B.S. and M.S. degrees in Electrical and Computer Engineering, and the Ph.D. degree in Applied Science, from the University of California at Davis, in 1985, 1986, and 1997, respectively. From 1986 to 1993 he was a Senior Engineer with Hughes Missile Systems Company (formerly General Dynamics Convair Division) in San Diego, CA. At Hughes, Dr. White was involved with inverse synthetic aperture radar imaging, radar target identification, and low-observables technology. In 1993 he joined Lawrence Livermore National Laboratory, where he is currently Group Leader of the Computational Engineering Group of the Defense Sciences Engineering Division. His current research interests include higher-order

methods for computational electromagnetics, multi-physics simulations, and massively parallel computing.